HHS Public Access

Author manuscript

Dev Biol. Author manuscript; available in PMC 2017 July 15.

Published in final edited form as:

Dev Biol. 2016 July 15; 415(2): 296–305. doi:10.1016/j.ydbio.2015.12.020.

A quantitative method for defining high-arched palate using the Tcof1$^{+/-}$ mutant mouse as a model

Zachary R. Conley[1], **Molly Hague**[1], **Hiroshi Kurosaka**[1,2], **Jill Dixon**[3], **Michael J. Dixon**[3,4], and **Paul A. Trainor**[1,5,*]

[1]The Stowers Institute for Medical Research, Kansas City, Missouri, United States of America

[2]Osaka University, Department of Orthodontics and Dentofacial Orthopedics, Graduate School of Dentistry, Osaka, Japan

[3]Manchester Academic Health Sciences Centre, Faculty of Medical and Human Sciences, Manchester, UK

[4]University of Manchester, Faculty of Life Sciences, Manchester, UK

[5]University of Kansas Medical Center, Kansas City, Kansas, United States of America

Abstract

The palate functions as the roof of the mouth in mammals, separating the oral and nasal cavities. Its complex embryonic development and assembly poses unique susceptibilities to intrinsic and extrinsic disruptions. Such disruptions may cause failure of the developing palatal shelves to fuse along the midline resulting in a cleft. In other cases the palate may fuse at an arch, resulting in a vaulted oral cavity, termed high-arched palate. There are many models available for studying the pathogenesis of cleft palate but a relative paucity for high-arched palate. One condition exhibiting either cleft palate or high-arched palate is Treacher Collins syndrome, a congenital disorder characterized by numerous craniofacial anomalies. We quantitatively analyzed palatal perturbations in the Tcof1$^{+/-}$ mouse model of Treacher Collins syndrome, which phenocopies the condition in humans. We discovered that 46% of Tcof1$^{+/-}$ mutant embryos and new born pups exhibit either soft clefts or full clefts. In addition, 17% of Tcof1$^{+/-}$ mutants were found to exhibit high-arched palate, defined as two sigma above the corresponding wild-type population mean for height and angular based arch measurements. Furthermore, palatal shelf length and shelf width were decreased in all Tcof1$^{+/-}$ mutant embryos and pups compared to controls. Interestingly, these phenotypes were subsequently ameliorated through genetic inhibition of p53. The results of our study therefore provide a simple, reproducible and quantitative method for investigating models of high-arched palate.

*Author for Correspondence: Paul A Trainor, Phone: 816 926 4414, pat@stowers.org.

Disclosures.

The authors declare no conflict of interest.

Keywords

high-arched palate; cleft palate; palatogenesis; quantitative imaging; Tcof1; Treacher Collins syndrome; mouse model

Introduction

During early mammalian embryo development, five facial prominences surround the primitive oral opening. These include the frontonasal prominence, maxillary prominences, and mandibular prominences. The frontonasal prominence is subsequently partitioned into medial and lateral nasal processes, followed by fusion between the medial nasal and maxillary prominences, leading to formation of rudimentary primary and secondary palatal shelves. The bilateral shelves of the secondary palate then grow vertically, beside the tongue in approximate synchrony with one another. The vertical shelves then undergo a reorientation above the tongue, grow horizontally towards each other, contact, adhere and fuse at the midline. As a part of the fusion process, a midline epithelial seam forms and disintegrates resulting in confluence of the palatal mesenchyme. This process is thought to collectively involve, convergence, extrusion, epithelial mesenchymal transformation and cell death. The full roof of the oral cavity is then completed through anterior fusion between the primary palate and secondary palate and anteriodorsal fusion between the secondary palate and nasal septum (Bush and Jiang, 2012).

Approximately one-third of all congenital birth disorders comprise craniofacial anomalies, many of which are classified as neurocristopathies since they are thought to arise via perturbations in neural crest cell development throughout embryogenesis (Trainor, 2003). Although a broad spectrum of craniofacial anomalies occur, the majority involve the palate and upper lip in the form of clefting. Cleft lip and/or palate is estimated to affect 1 in 700 live births, and is influenced by genetic factors and environmental exposures, as well as racial background, socioeconomic status, and geography (Dixon et al., 2011). Interestingly, about 70% of cleft lip with or without cleft palate cases and about 50% of cleft palate cases occur as isolated, “non-syndromic” cases. Non-syndromic cases of human CLP can include such subclinical phenotypes as lip pits and/or prints (Neiswanger et al., 2009), dental defects (Vieira et al., 2008), or even perturbations of the orbicularis oris muscle (Neiswanger et al., 2007; Weinberg et al., 2008). Orofacial clefts are associated with early-life complications include feeding and ear infections (Narayanan et al., 2013). Furthermore, affected children are also at a greater risk for oral health problems including dental caries, gingival health, malocclusion, and oral mucosal health (Chopra et al., 2014). Thus orofacial clefts are associated with both functional and aesthetic challenges.

In addition to cleft palate, high-arched palate (also described as “pseudo-cleft” or “vaulted palate”) represents another example of perturbed palatogenesis and is known to occur in ciliopathy-related syndromes (Tabler et al., 2013). High-arched palate, a phenotype for which the etiology is still unclear, manifests itself with an abnormally pronounced curvature angled superiorly along the palatal midline. The high-arched palate is associated with postnatal gingival swelling, crowding in the molars, and other such secondary dental

anomalies. As a result, affected individuals may experience speech impairments and difficulties in intubation (Tabler et al., 2013). Thus, high-arched palate is a significant factor in patient quality of life. Owing to its association with complex syndromes, high-arched palate has received some attention in the clinical literature, however this condition remains understudied due to a paucity of relevant models for investigating the etiology and pathogenesis of high-arched palate.

In humans, the process of palatogenesis begins during week 6 of gestation and is completed by around 12 weeks. In comparison, palatogenesis in mice begins around embryonic day (E) 11.5 and is typically complete by E16 or 17 (Bush and Jiang, 2012). Here, we describe the cleft and high-arched palate phenotypes of Tcof1$^{+/-}$ mutant mice, which mimic similar craniofacial anomalies characteristic of Treacher Collins syndrome. More importantly, we have developed a simple, yet consistent and reproducible method for quantifying arching and we define high-arched palate as two standard deviations above the wild-type arch height and arch angle means. Collectively, our results can be broadly applied to further understand the etiology and pathogenesis of high-arched palate.

Materials and methods

Mice

The Institutional Animal Care and Use Committee of The Stowers Institute for Medical Research approved all animal protocols used in this study. We bred congenic DBA Tcof1$^{+/-}$ mice with C57BL/6 wild-type mice to generate mixed DBA x C57BL/6 F_1 progeny as previously described (Dixon et al., 2000; Dixon and Dixon, 2004; Dixon et al., 2006). We additionally bred congenic DBA-Tcof1$^{+/-}$ mice with Trp53+/− on a C57BL/6 background to generate compound Tcof1$^{+/-}$;Trp53$^{+/-}$ mice as previously described (Jones et al., 2008). Embryos were obtained via timed mating, with the morning of detection of a vaginal plug being designated embryonic day (E)0.5. Tissue samples from individual progenitor embryos or pups were collected and genotyped through Transnetyx Inc.

Nuclear fluorescent imaging

The heads of aforementioned mutant and wild-type F_1 progeny were fixed in 4% paraformaldehyde overnight at 4°C. Whole fixed samples were washed several times in PBS before mandibles were removed to expose the palate. Palate samples were stained directly with DAPI (Sigma-Aldrich) in PBS and subsequently imaged using an LSM-700 Upright confocal microscope as previously described (Sandell et al., 2012).

Image analysis

Maximum intensity projections were obtained from complete z-stack sets of palate samples using the ZEN microscope software. 3-D rendering of full z-stacks was performed through Imaris software (Bitplane, Zurich, Switzerland). Coordinate data from orthogonal views including Z-profiles were obtained using ImageJ 1.48 bundled with 64-bit Java (Rasband, 1997–2012) (Supp. Info. Movies S1–S3).

Palate arch height measurements were obtained from Z-profiles via calculating the shortest distance from the highest superior point of the palate (Supp. Info. Fig. S1A–D, red point P_0) to the line representing the lateral base of the palate shelves (red line passing through points P_1 and P_2):

$$\text{distance}\,(P_1, P_2, (x_0, y_0)) = \frac{(y_2-y_1)x_0-(x_2-x_1)y_0+x_2y_1-y_2x_1}{\sqrt{(y_2-y_1)^2+(x_2-x_1)^2}}$$

Palate arch degree measurements were obtained from aforementioned Z-profiles via calculating θ_1 of angle $<P_0P_1P_2$ and θ_2 of angle $<P_0P_2P_1$. In each sample, θ_1 and θ_2 were averaged (θ_f) for final data sets used in statistical measurements (Supp. Info. Fig. S1D):

$$\theta_1 = \deg\left[\arccos\left(\frac{p_{12}2+p_{02}2-p_{01}2}{2\cdot(p_{12}\cdot p_{02})}\right)\right]$$
$$\theta_2 = \deg\left[\arccos\left(\frac{p_{12}2+p_{01}2-p_{02}2}{2\cdot(p_{12}\cdot p_{01})}\right)\right]$$
$$\theta_f = \frac{\theta_1+\theta_2}{2}$$

Histology

Embryos were dissected in PBS, fixed in 4% paraformaldehyde overnight at 4°C, and stored in 70% ethanol. Embryo heads were separated from their bodies, embedded in paraffin, sectioned coronally, and stained with hematoxylin and eosin, or immunostained with HHF35, an anti-muscle actin antibody, prior to imaging. Coronal sections in Fig. 3 and Supplementary Information. Fig. 2S, were prepared in accordance with a previously published staging description (Yu and Ornitz, 2011).

Statistics

One-tailed Student's t tests were performed on data sets for palate shelf length, shelf width, arch height, and arch angles. One-way analysis of variance with Bonferroni post hoc corrections were performed on aforementioned independent parameters of the three groups of the rescue data set with IBM SPSS Statistics. P values of less than 0.05 were considered significant.

Results

Tcof1$^{+/-}$ mutant mice exhibit perturbed palatogenesis, including cleft palate, during development

Previously, we demonstrated that Tcof1$^{+/-}$ mice phenocopy Treacher Collins syndrome in humans including the presence of cleft palate (Dixon et al., 2006). Mechanistically, this is thought to arise due to elevated neuroepithelial apoptosis and diminished numbers of migrating neural crest cells which leads to hypoplasia of the lateral and medial facial prominences as well as the maxillary and mandibular components of the first pharyngeal arch (Dixon et al., 2006). At birth Tcof1$^{+/-}$ mice exhibit smaller, domed heads together with micophthalmia or anophthalmia compared to wild-type littermates (Fig. 1A–F). The onset of

these craniofacial anomalies is profoundly evident even in E13.5 embryos by the stunted development of the nasal, frontal, maxilla, premaxilla, and mandibular regions (Fig. 1A–F).

Here, we expound on the observation that humans with Treacher Collins syndrome often exhibit high-arched palate, hypothesizing that we could utilize Tcof1$^{+/-}$ mice as a model for exploring and quantifying the temporal dynamics of high-arched palate pathogenesis. E12.5 to E18.5 wild-type control and Tcof1$^{+/-}$ embryos were collected, fixed, DAPI stained, and imaged via confocal microscope to obtain Z-stacks transversally spanning entire palates (Fig. 2). Obliquely directed grooves appeared less defined in the E12.5 mutant than in the wild-type counterparts (compare Fig. 2A with Fig. 2H). In E13.5 embryos, it was generally clear that the length of the palate shelves of Tcof1$^{+/-}$ mutants appeared to be grossly stunted relative to control littermates (compare vertical white lines in Figs. 2B and 2I) and also that the developing rugae in Tcof1$^{+/-}$ mutants at this stage appeared thicker and noticeably more asymmetric. At E14.5, palatal fusion in Tcof1$^{+/-}$ embryos lagged behind their wild-type counterparts, resulting in the palatal shelves appearing further separated than in controls (Fig. 2D, K). By E15.5 cleft palate was evident in some Tcof1+/− embryos (Fig. 2E, L), whereas by E17.5 the Tcof1$^{+/-}$ embryos in which the palatal shelves completed fusion displayed a high-arched palate (Figs. 2F, M). In these late stage embryos, depressions existed along the midline epithelial seam, which was not detected in wild-type controls.

The phenotype of Tcof1$^{+/-}$ embryos has been attributed to diminished numbers of migrating neural crest cells and subsequent hypoplasia of the facial prominences. Consistent with this idea, comparative coronal sections of wild-type and Tcof1$^{+/-}$ embryos revealed that the mutants exhibit noticeable hypoplasia of the palatal shelves during the vertical growth phase at E12.5 (Fig. 3). Furthermore, horizontal growth at E14.5 appears to be perturbed, while by E16.5, Tcof1$^{+/-}$ embryos exhibit elevated and more curved oral roofs (Fig. 3). The palate images shown in Figures 2 and 3 represent typical cases and not necessarily the most severe phenotype.

Interestingly, neural crest cells are known to play an important role in facial muscle patterning (Noden, 1983; Noden and Trainor, 2005), and furthermore, cleft palate and high-arched palate phenotypes are often accompanied by sub-clinical phenotypes including perturbation of the facial muscles, particularly the orbicularis oris muscle (Neiswanger et al., 2007). Our examination of facial muscle composition via immunostaining with the muscle marker HH35, revealed a general hypoplasia of the masseter (ma), extra orbital (eom), glossogenial (g), and anterior digastric (ad) muscles in Tcof1$^{+/-}$ embryos compared to wild-type littermates (Supp. Info. Fig. S2). Functionally this may affect the ability of newborn Tcof1$^{+/-}$ pups to suckle properly.

In viewing coronal histological sections of the head, we also observed significant obstruction of the nasal cavity (nc) (Supp. Info. Fig. S3). Thus Tcof1$^{+/-}$ embryos exhibit perturbation of palate and nasal development in association with abnormalities of craniofacial muscle patterning, each of which is likely to contribute to the perinatal lethality of Tcof1$^{+/-}$ pups.

Approximately 46% of Tcof1$^{+/-}$ mice mutant mice exhibit either soft or full cleft palate

In order to understand the frequency with which Tcof1$^{+/-}$ mice exhibit cleft palate, a total of 12 timed litters of mice generating 79 total embryos and pups were examined between E18.5 – P0.5 (Fig. 4). Of the 35 Tcof1$^{+/-}$ mutants, 40% (n = 14), displayed soft palate clefts (clefts restricted to the soft, muscular tissue of the back of the roof of the oral cavity, Fig. 4A, B, D, E) whereas 6% (n = 2), presented with full clefts (compound clefts extending from the hard, secondary palate to the soft palate (Figs 4A, C, D, F).

Tcof1$^{+/-}$ mice exhibit increased palate arch heights and arch angles together with reductions in palatal shelf length and width

A significant fraction of fused Tcof1$^{+/-}$ mutant palates appeared to be higher and more arched than their wild-type counterparts when viewed three dimensionally as volume-rendered optical projections of full-Z confocal image stacks (Supp. Info. Movies S1, 2). In an effort to establish a quantitative diagnostic criteria for high-arched palate, we measured palate arch height (defined as the shortest distance in-between the highest superior point of the palate and, in the same plane, the line delineating the lowest lateral surface of the palate base) for the aforementioned 79 embryos (Fig. 5; Supp. Info. Fig. S1). From the 44 wild-type specimens, we recorded an average palate arch height of 362 μM (± 59 μM) with a median of 364 μM (Fig. 5A). In comparison, from 33 Tcof1$^{+/-}$ mutant specimens, the average palate arch height was considerably higher at 392 μM (± 81 μM) with a median of 378 μM (Fig. 5B).

In addition to palate arch height as a measure for the extent of arching, we also calculated the angle between the palate surface and a reference line connecting each respective palatal shelf to the highest point of the palate arch (Supp. Info. Fig. S1). Due to natural asymmetric variations in palatal development, such angles within a single sample are close in value to one another but are not identical. Thus, angle values in represented data sets exist as an average of both aforementioned angle values for each sample. The average angle for all wild-type samples in the control group was 18.7 degrees (± 2.5) while the average for Tcof1$^{+/-}$ embryos and pups was 22.6 (± 3.1) degrees (Fig. 5C, D). The difference in both palate arch height and palate arch angle between wild-type and Tcof1$^{+/-}$ mutants was statistically significant.

In addition to the palates of Tcof1$^{+/-}$ embryos appearing to exhibit significant differences in the Z-plane compared to littermate controls, we also determined there were marked differences in the length and width of the palate shelves. Palate shelf length was measured from the superior nasal septum landmark to the posterior vibrating line border (Supp. Info. Fig. S1). The average palate shelf length was found to be 2573.4 μM (± 167.4 μM) and 1948.1 μM (± 269.8 μM) for wild-type and Tcof1$^{+/-}$ mutants, respectively (Fig. 5E, F). In order to calculate palate shelf width, we measured the distance delineated by the lateral edge of the palate shelf and the midline epithelial seam. The average palate shelf width for wild-type mice and Tcof1$^{+/-}$ mutants was 1336.5 μM (± 65.9 μM) and 1227.3 μM (± 98.6 μM) respectively (Fig. 5G, H). The decrease in both palate shelf length and palate shelf width in Tcof1$^{+/-}$ mutants compared to wild-type controls was statistically significant.

Tcof1$^{+/-}$ mutant mice exhibit high-arched palate

We defined Tcof1$^{+/-}$ mutant mice with palate arch heights and angles that were at least two standard deviations above the wild-type mean as being high-arched. Thus, the diagnostic cutoffs for palate arch height and palate arch angle were 480.3 μM and 23.6 degrees, respectively. The top 6 and 12 samples from the palate arch height and arch angle data sets, respectively, exceeded the diagnostic cutoffs within their measurement groups. All six samples containing palate arch height measurements above the diagnostic cutoff also met the corresponding palate arch angle measurement cutoff and were thus deemed high-arched. Thus, 6 out of a total 35 (17%) Tcof1$^{+/-}$ mutants met our criteria for being defined as having a high-arched palate (Fig. 6). Oral views of DAPI stained (Fig. 6A, C–F) and optical Z-profiles (Fig. 6G, I–L) of a wild-type control and four such high-arched palate samples along with their graphical location in respectively ranked data sets for palate shelf height are shown (Fig. 6M, N). When comparing the Z-profiles of high-arched palates to that of an average mutant (Fig. 6B, H), the difference in palate shelf height and angle are significant enough to be qualitatively perceived in each case. Thus we have established a simple yet consistent and reproducible, quantitative method for defining the phenotype of high-arched palate

Tcof1$^{+/-}$ mutant palate phenotypes are rescued by genetic knockout of Trp53

We have previously shown that craniofacial defects in Tcof1$^{+/-}$ mutant mice are due to p53 dependent neuroepithelial apoptosis and diminishment of migrating neural crest cells (Jones et al., 2008). Furthermore, we also explored the potential for p53 inhibition as a therapeutic avenue for preventing Treacher Collins. Indeed, p53 inhibition suppresses cyclin G1-driven neuroepithelial cell death leading to the generation of appropriate numbers of migrating neural crest cell, which in turn leads to proper craniofacial development and post-natal viability (Jones et al., 2008). To date, the effect of p53 inhibition specifically on palatal development in Tcof1$^{+/-}$ mutant mice has not been analyzed. We therefore collected 23 wild-type (Tcof1$^{+/+}$;Trp53$^{+/+}$), 16 Tcof1$^{+/-}$ (Tcof1$^{+/-}$;Trp53$^{+/+}$) and 19 compound heterozygote (Tcof1$^{+/-}$;Trp53$^{+/-}$) embryos and pups between E18.5 and P0.5 (Figs. 7, 8; Supp. Info. Movies S1–3).

Zero cases of cleft palate, neither soft nor full, were found in any mutant embryo or mouse from these crosses. The absence of cleft palate in Tcof1$^{+/-}$ embryos and mice born to Trp53$^{+/-}$ mothers in contrast to Tcof1$^{+/-}$ offspring from wild-type mothers was surprising. Nonetheless, in order to analyze the effect of p53 haploinsufficiency on the Tcof1$^{+/-}$ mutant palate, palate arch heights, angles, lengths, and widths were measured in the same way as previously described (Supp. Info. Fig. S1). The resultant mean palate arch heights were 392.5 μM (± 77.8 μM), 403.2 μM (± 64.4 μM), and 405.5 μM (± 84.6 μM) for wild-type, Tcof1$^{+/-}$, and Tcof1^{+-};Trp53$^{+/-}$ groups, respectively (Fig. 8A–B). Mean palate arch degree values were 19.5 degrees (± 3.2), 21.3 degrees (± 3.5), and 20.1 degrees (± 4.1) for wild-type, Tcof1$^{+/-}$, and Tcof1$^{+/-}$;Trp53$^{+/-}$ groups, respectively (Fig. 8 C–D). Mean palate arch length values were 2692.1 μM (± 157.9 μM), 2139.8 μM (± 255 μM), and 2544.9 μM (± 229.9 μM) for wild-type, Tcof1$^{+/-}$, and Tcof1$^{+/-}$;Trp53$^{+/-}$ groups, respectively (Fig. 8E, F). Differences in palate arch length between wild-type and Tcof1$^{+/-}$, as well as between Tcof1$^{+/-}$ and Tcof1$^{+/-}$;Trp53$^{+/-}$ were statistically significant. Lastly, mean palate arch width

values were 1344.9 μM (± 100 μM), 1276.6 μM (± 136.487 μM), and 1341.2 μM (± 115.3 μM) for wild-type, Tcof1$^{+/-}$, and Tcof1$^{+/-}$;Trp53$^{+/-}$ groups, respectively (Fig. 8G, H). Representatives of samples around the mean values for palate arch measurements are represented in Figure 7. Thus, similar to its effect in restoring proper craniosketal development and post-natal viability (Jones et al., 2008), inhibition of p53 can also restore palatal shelf length to normal in Tcof1$^{+/-}$ mice, while also partially normalizing palatal shelf width and palate angle.

Discussion

Orofacial clefts are collectively the most common craniofacial birth defect observed in humans (Rahimov et al., 2012). These structural anomalies require extensive medical and behavioral interventions, imposing significant personal and economic burden on patients and their affected families (Wehby and Cassell, 2010). Although many models of facial clefts have been generated and described, there are few models of high-arched palate development. The Tcof1$^{+/-}$ mouse which mimics Treacher Collins syndrome may serve as a useful model for understanding the pathogenesis of high-arched palate. However, before that can happen, a consistent and reliable method is needed to reproducibly quantify high-arched palate.

Our analysis of palatogenesis in Tcof1$^{+/-}$ mice showed that Tcof1$^{+/-}$ haploinsufficiency leads to cleft palate in 46% of cases. This is in comparison with a frequency of 28% in humans with Treacher Collins syndrome (Katsanis and Jabs, 1993–2015). Moreover, our work defines an accurate, consistent and reproducible methodology for measuring key palatogenesis metrics such as palatal shelf length, width, height and angle. Utilizing such metrics, we demonstrated that Tcof1$^{+/-}$ mouse embryos and pups exhibit significantly reduced palate shelf lengths and widths compared to wild-type littermate controls. Moreover, utilizing metrics for both palate arch height and angle, we discovered that Tcof1$^{+/-}$ mutants had significantly increased values in both cases, especially in angle measurements. Tcof1$^{+/-}$ mutants with both arch height and arch angle values, exceeding two standard deviations above their corresponding wild-type controls, existed within the set and were thus termed high-arched palate. Two standard deviations above the mean normative score is a commonly used clinical indicator of abnormality (Grimberg and Lifshitz, 2007).

Palate differences were much more significant with respect to arch angle measurements than in the length measurements. It is worth noting that natural asymmetries in temporal embryonic growth, both between litters and within individual litters, seem to account for potentially large differences in palatal size and, thus, do pose a noise limitation in data sets. Palate arch angle measurements remove noise associated with aforementioned growth asymmetries, instead providing information more sensitive to the morphology and shelf perturbation in the high-arched phenotype. It seems the higher the angle value in palate arch angle measurements, the greater the exertion of the hypoplastic mutant palate in order to achieve fusion. We noticed that, in some cases of high-arched palate, tissue along the midline epithelial seam appeared depressed relative to the rest of the palate. A logical route for a hypoplastic palate to achieve contact at an arch would be one in which an increase in total surface area is traded for decreased tissue thickness.

Tcof1 is broadly expressed during embryogenesis and functions as a positive regulator of ribosome biogenesis, promoting cell proliferation (Dixon et al., 2006). Although, Tcof1 is important in many cell types, previous analyses have demonstrated that Tcof1 haploinsuffiency primarily affects neuroepithelial and neural crest cell viability and proliferation. Moreover, neuroepithelial and neural crest cells appear to be especially vulnerable to stress (Nonn et al., 2003). This particular sensitivity in neuroepithelial and neural crest cells is widely considered to contribute to the frequency of birth defects, since neural crest cell-related craniofacial anomalies comprise approximately one third of all congenital anomalies. Interestingly, genetic inhibition of p53 suppresses apoptosis in $Tcof1^{+/-}$ mutant mice, ameliorating the characteristic craniofacial abnormalities (Jones et al., 2008). In accordance with this data, we observed a rescue or normalization of palate shelf length, width, and arch angle in $Tcof1^{+/-}$;$Trp53^{+/-}$ embryos, parameters which are perturbed in $Tcof1^{+/-}$ embryos due to a decreased number of neural crest cells contributing to the palatal mesenchyme. Unexpectedly, we found a surprising absence of facial clefts in $Tcof1^{+/-}$ embryos when the mother was $Trp53^{+/-}$, although these embryos still continued to exhibit severe nasal cavity malformations (Fig. S3). While it may be tempting to speculate that the $Trp53^{+/-}$ maternal background may have some potentially palate-specific protective effect, such a conclusion cannot be drawn without quantitative analyses of embryos derived from the reciprocal breeding cross, where the father is $Trp53^{+/-}$. However, in crossing a $Trp53^{+/-}$, father to a $Tcof1^{+/-}$ mother we would also need to consider the possibility of a protective or detrimental effect from the maternal environment of a $Tcof1^{+/-}$ mother Furthermore, the unexpected phenotype may simply be a consequence of other developmental effects. Nonetheless this phenomenon warrants further exploration in the future.

In conclusion, the results of our study are significant for further mechanistic examination of palatal defects, most compellingly those of a high-arched palate phenotype. Our quantitative demonstration of the presence of high-arched palate in Tcof1 mutants and subsequent p53 amelioration, strongly suggests a link between cranial neural crest cell induced tissue and palatal shelf hypoplasia, and the pathogenesis of high-arched palate. Furthermore, examination of the high-arched palate phenotype in the $Tcof1^{+/-}$ mouse model of Treacher Collins syndrome indicates that the pathology underlying this phenotype in this and possibly other associated conditions may be different from that shown to arise in ciliopathy related syndromes (Tabler et al., 2013). Fuz mice for example exhibit increased numbers of neural crest cells and elevated Fgf8 signaling as part of a ciliopathy condition. In contrast $Tcof1^{+/-}$ mice exhibit a deficiency in the number of migrating neural crest cells in association with neuroepithelial cell death as part of a ribosomopathy condition. Despite these differences both Fuz and $Tcof1^{+/-}$ mutants exhibit high-arched palate as part of their craniofacial phenotype. Hence it appears very distinct mechanisms may lead to the same phenotype, although this still remains to be formally proven.

In conclusion, the primary goal of our study was to establish a platform with which to quantitatively and reproducibly define high-arched palate in any mouse model of palate dysmorphogenesis. It is our intention now to use this approach to identify and characterize $Tcof1^{+/-}$ mice on different backgrounds (see Dixon et al., 2004) which exhibit a high penetrance of either high-arched palate or cleft palate, but not both, so that we can begin to

address whether high-arched palate and cleft palate maybe in some cases part of a phenotypic spectrum, or whether their mechanistic pathogenesis is different. It will also be very interesting to use this approach to determine whether there is a correlation between palate length or width with cleft or high-arched palates, which may address the question of whether constraint imposed by the maxilla is a cause of palate dysmorphogenesis. Thus our quantitative analyses set the stage for exploring these questions in the future and for also defining the presence of high-arched palate in mouse models of perturbed palatogenesis.

Supplementary Material

Refer to Web version on PubMed Central for supplementary material.

Acknowledgments

Research in the Trainor laboratory is supported by the Stowers Institute for Medical Research, and National Institute of Dental and Craniofacial Research (R01 DE 016082).

References

Bush JO, Jiang R. Palatogenesis: morphogenetic and molecular mechanisms of secondary palate development. Development. 2012; 139:231–243. [PubMed: 22186724]

Chopra A, Lakhanpal M, Rao NC, Gupta N, Vashisth S. Oral health in 4–6 years children with cleft lip/palate: a case control study. North American journal of medical sciences. 2014; 6:266–269. [PubMed: 25006561]

Dixon J, Brakebusch C, Fassler R, Dixon MJ. Increased levels of apoptosis in the prefusion neural folds underlie the craniofacial disorder, Treacher Collins syndrome. Hum Mol Genet. 2000; 9:1473–1480. [PubMed: 10888597]

Dixon J, Dixon MJ. Genetic background has a major effect on the penetrance and severity of craniofacial defects in mice heterozygous for the gene encoding the nucleolar protein Treacle. Dev Dyn. 2004; 229:907–914. [PubMed: 15042714]

Dixon J, Jones NC, Sandell LL, Jayasinghe SM, Crane J, Rey JP, Dixon MJ, Trainor PA. Tcof1/Treacle is required for neural crest cell formation and proliferation deficiencies that cause craniofacial abnormalities. Proc Natl Acad Sci U S A. 2006; 103:13403–13408. [PubMed: 16938878]

Dixon MJ, Marazita ML, Beaty TH, Murray JC. Cleft lip and palate: understanding genetic and environmental influences. Nature reviews Genetics. 2011; 12:167–178.

Grimberg, A.; Lifshitz, F. Worrisome Growth. In: Lifshitz, F., editor. Pediatreic Endocrinology: Growth, Adrenal, Sexual, Thyroid, Calcium and Fluid Balance Disorders. Informa Helathcare; New York, NY: 2007. p. 1-50.

Jones NC, Lynn ML, Gaudenz K, Sakai D, Aoto K, Rey JP, Glynn EF, Ellington L, Du C, Dixon J, Dixon MJ, Trainor PA. Prevention of the neurocristopathy Treacher Collins syndrome through inhibition of p53 function. Nat Med. 2008; 14:125–133. [PubMed: 18246078]

Katsanis, SH.; Jabs, EW. Treacher Collins Syndrome. Pagon, RA.; Adam, MP.; Ardinger, HH.; Wallace, SE.; Amemiya, A.; Bean, LJH.; Bird, TD.; Fong, CT.; Smith, RJH.; Stephens, K., editors. GeneReviews(R); Seattle (WA): 1993–2015.

Narayanan DS, Pandian SS, Murugesan S, Kumar R. The incidence of secretory otitis media in cases of cleft palate. Journal of clinical and diagnostic research : JCDR. 2013; 7:1383–1386. [PubMed: 23998070]

Neiswanger K, Walker K, Klotz CM, Cooper ME, Bardi KM, Brandon CA, Weinberg SM, Vieira AR, Martin RA, Czeizel AE, Castilla EE, Poletta FA, Marazita ML. Whorl patterns on the lower lip are associated with nonsyndromic cleft lip with or without cleft palate. American journal of medical genetics Part A. 2009; 149A:2673–2679. [PubMed: 19921634]

Neiswanger K, Weinberg SM, Rogers CR, Brandon CA, Cooper ME, Bardi KM, Deleyiannis FW, Resick JM, Bowen A, Mooney MP, de Salamanca JE, Gonzalez B, Maher BS, Martin RA, Marazita ML. Orbicularis oris muscle defects as an expanded phenotypic feature in nonsyndromic cleft lip with or without cleft palate. American journal of medical genetics Part A. 2007; 143A: 1143–1149. [PubMed: 17497721]

Noden DM. The role of the neural crest in patterning of avian cranial skeletal, connective, and muscle tissues. Dev Biol. 1983; 96:144–165. [PubMed: 6825950]

Noden DM, Trainor PA. Relations and interactions between cranial mesoderm and neural crest populations. J Anat. 2005; 207:575–601. [PubMed: 16313393]

Nonn L, Williams RR, Erickson RP, Powis G. The absence of mitochondrial thioredoxin 2 causes massive apoptosis, exencephaly, and early embryonic lethality in homozygous mice. Mol Cell Biol. 2003; 23:916–922. [PubMed: 12529397]

Rahimov F, Jugessur A, Murray JC. Genetics of nonsyndromic orofacial clefts. Cleft Palate Craniofac J. 2012; 49:73–91. [PubMed: 21545302]

Rasband, WS. Image J. U.S. National Institutes of Health; Bethesda, Marlyand, USA: 1997–2012. imaagej.nih.gov/ij/

Sandell LL, Kurosaka H, Trainor PA. Whole mount nuclear fluorescent imaging: convenient documentation of embryo morphology. Genesis. 2012; 50:844–850. [PubMed: 22930523]

Tabler JM, Barrell WB, Szabo-Rogers HL, Healy C, Yeung Y, Perdiguero EG, Schulz C, Yannakoudakis BZ, Mesbahi A, Wlodarczyk B, Geissmann F, Finnell RH, Wallingford JB, Liu KJ. Fuz mutant mice reveal shared mechanisms between ciliopathies and FGF-related syndromes. Dev Cell. 2013; 25:623–635. [PubMed: 23806618]

Trainor PA. Making headway: the roles of Hox genes and neural crest cells in craniofacial development. ScientificWorldJournal. 2003; 3:240–264. [PubMed: 12806110]

Vieira AR, McHenry TG, Daack-Hirsch S, Murray JC, Marazita ML. Candidate gene/loci studies in cleft lip/palate and dental anomalies finds novel susceptibility genes for clefts. Genetics in medicine : official journal of the American College of Medical Genetics. 2008; 10:668–674. [PubMed: 18978678]

Wehby GL, Cassell CH. The impact of orofacial clefts on quality of life and healthcare use and costs. Oral Dis. 2010; 16:3–10. [PubMed: 19656316]

Weinberg SM, Brandon CA, McHenry TH, Neiswanger K, Deleyiannis FW, de Salamanca JE, Castilla EE, Czeizel AE, Vieira AR, Marazita ML. Rethinking isolated cleft palate: evidence of occult lip defects in a subset of cases. American journal of medical genetics Part A. 2008; 146A:1670–1675. [PubMed: 18536047]

Yu K, Ornitz DM. Histomorphological study of palatal shelf elevation during murine secondary palate formation. Dev Dyn. 2011; 240:1737–1744. [PubMed: 21618642]

Highlights

- Cleft palate is associated with functional and aesthetic challenges
- High-arched palate is an example of perturbed palatogenesis
- High-arched palate is also known as pseudo cleft or vaulted palate
- There is a paucity of models for investigating high-arched palate
- We established a quantitative method for defining high-arched palate

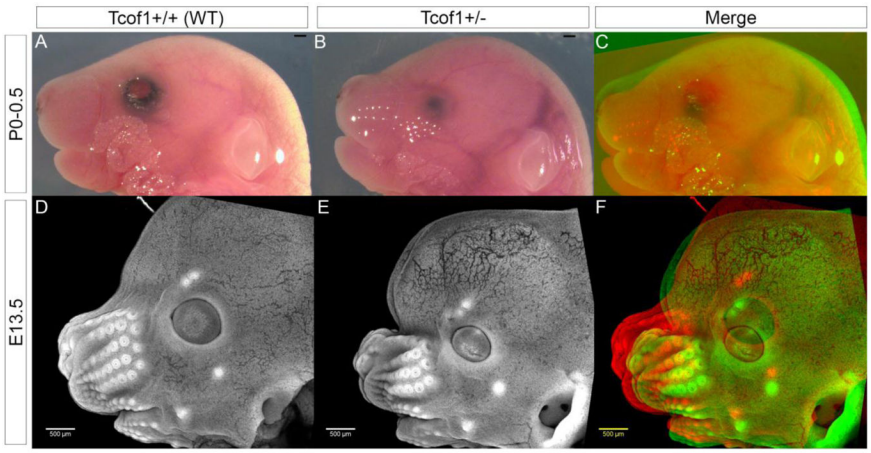

Figure 1.

Gross craniofacial images of wild-type control and Tcof1$^{+/-}$ pups and embryos. Bright field images of P0–0.5 (A) wild-type, (B) Tcof1$^{+/-}$, and (C) merged samples. DAPI-stained E13.5 (D) wild-type (E) Tcof1$^{+/-}$, and (F) merged samples. Scale bars are 500 μM.

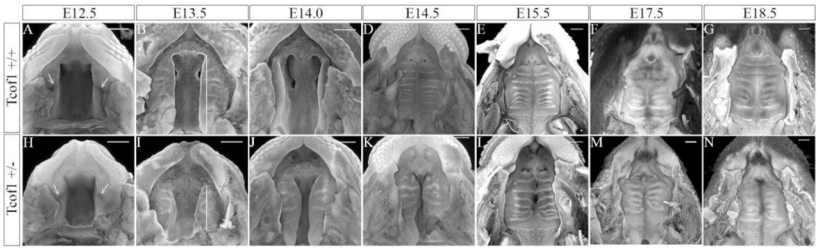

Figure 2.

Maximum intensity fluorescent confocal projection images of DAPI stained palates of representative stages of wild-type (A–F) and Tcof1$^{+/-}$ embryos (H–N). Arrows indicate location of obliquely directed grooves. Vertical white lines indicate palate shelf length. Scale bars are 500 μM.

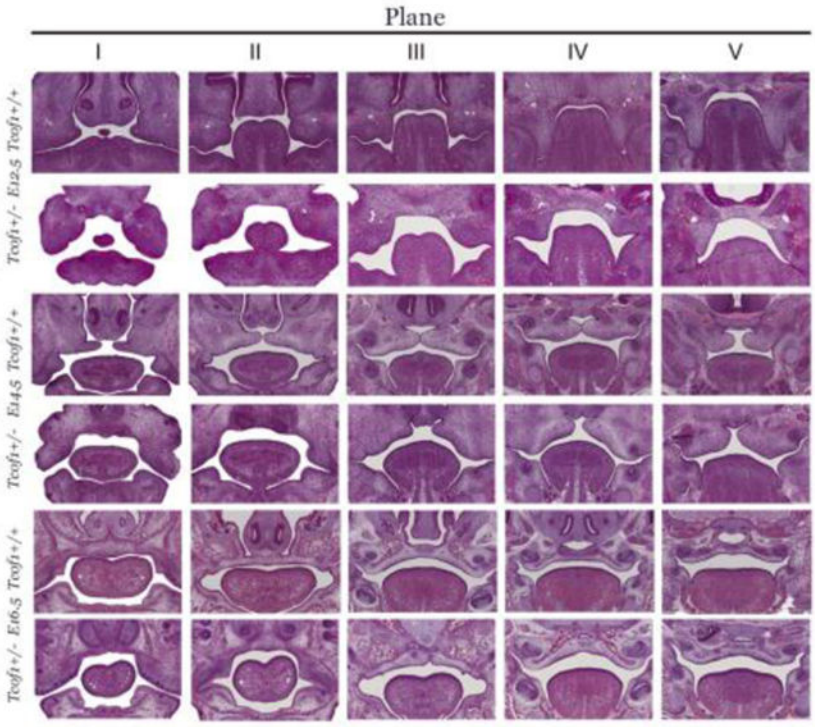

Figure 3.
Coronal histological sections of E12.5, E14.5 and E16.5 wild-type and Tcof1$^{+/-}$ mutants organized into five planes (I–V) moving anterior to posterior.

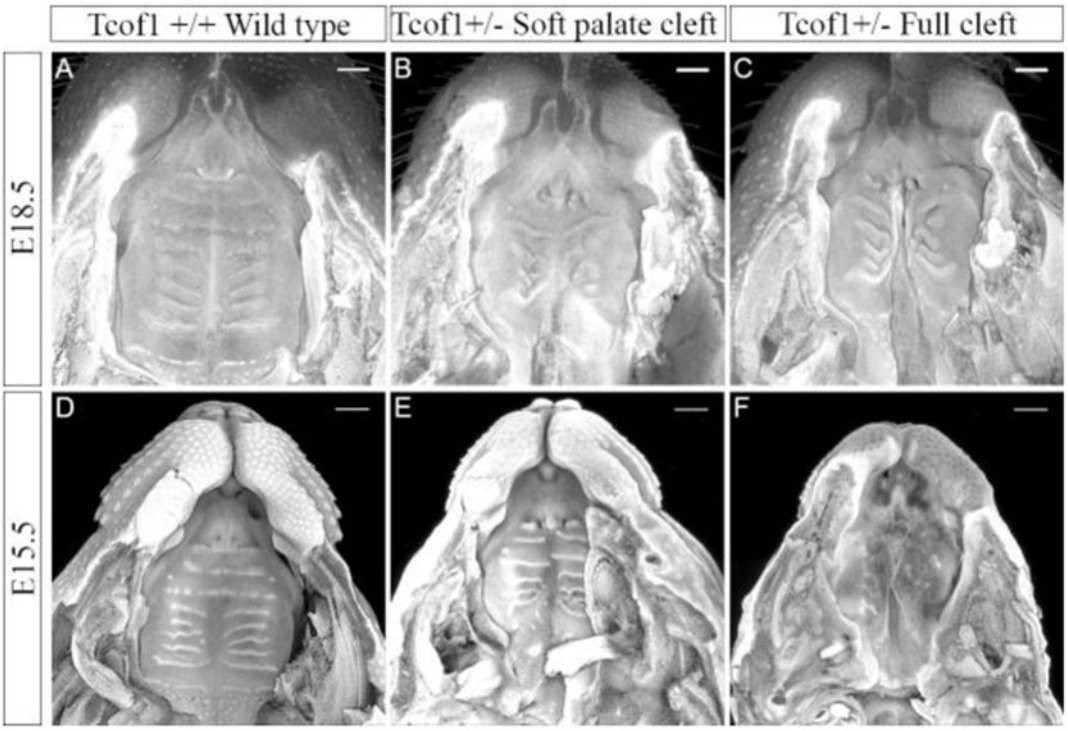

Figure 4.

Maximum intensity fluorescent confocal projection images of DAPI stained palates of wild-type (A, D) and either soft palate cleft (B and E) or full palate cleft (C and F) in Tcof1$^{+/-}$ embryos. Scale bars are 500 μM.

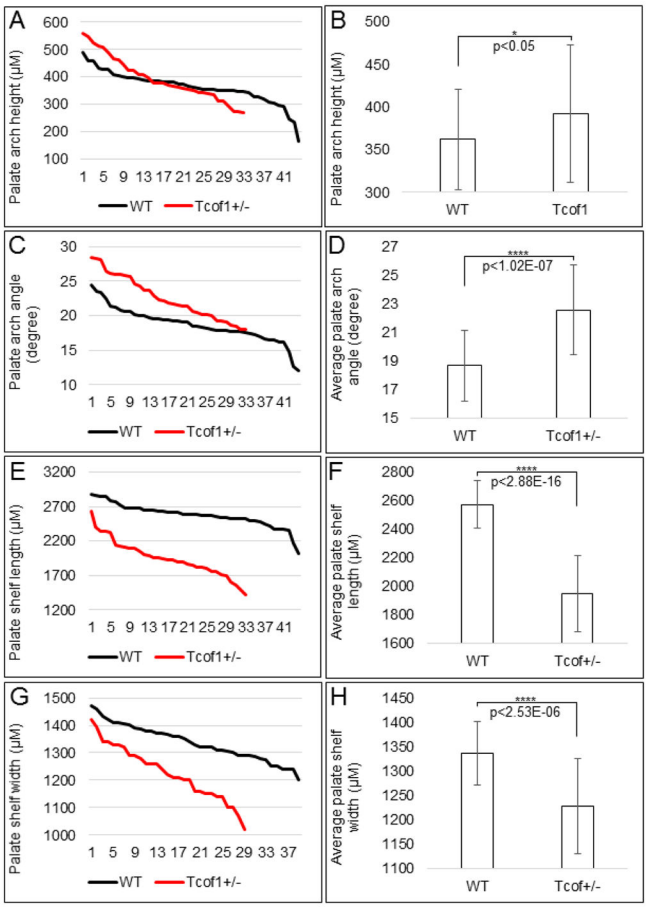

Figure 5.

Analyses of palate arch height (A, B), angle (C, D), shelf length (E, F), and shelf width (G, H) measurements in wild-type and Tcof1$^{+/-}$ embryos and pups. Samples were plotted from greatest to least magnitude (A, C, E, G). Bar graphs (B, D, F, H) represent the averages and standard deviations of wild-type and Tcof1$^{+/-}$ palate arch height, arch angle, shelf length, and shelf width sets, respectively.

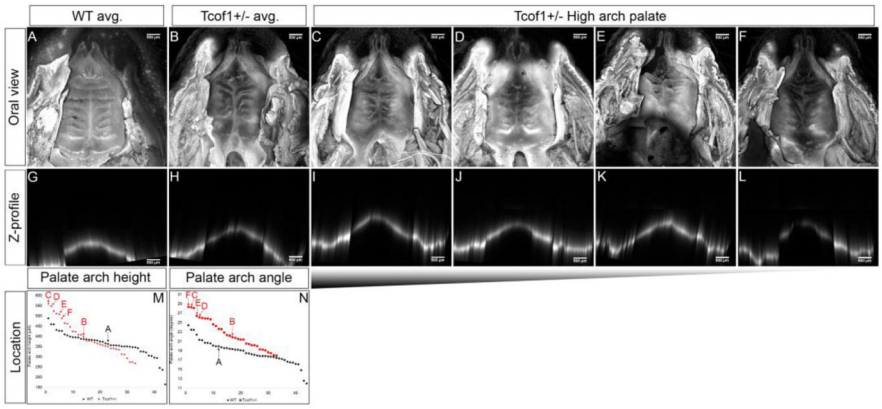

Figure 6.

Oral maximum intensity projections of DAPI-stained confocal Z-stacks of wild-type and Tcof1$^{+/-}$ (of approximately average palate arch height and angle) samples (A–F). Image of average high-arched palate inTcof1$^{+/-}$ embryos (B). (C–F) Similar views of Tcof1$^{+/-}$ high-arched palates, decreasing in severity. (G–L) Z-profiles of corresponding maximum intensity projections of embryos in A–F. (M–N) Sorted scatter plots of palate arch height and arch angle measurements, respectively, demarcating the locations of each represented sample.

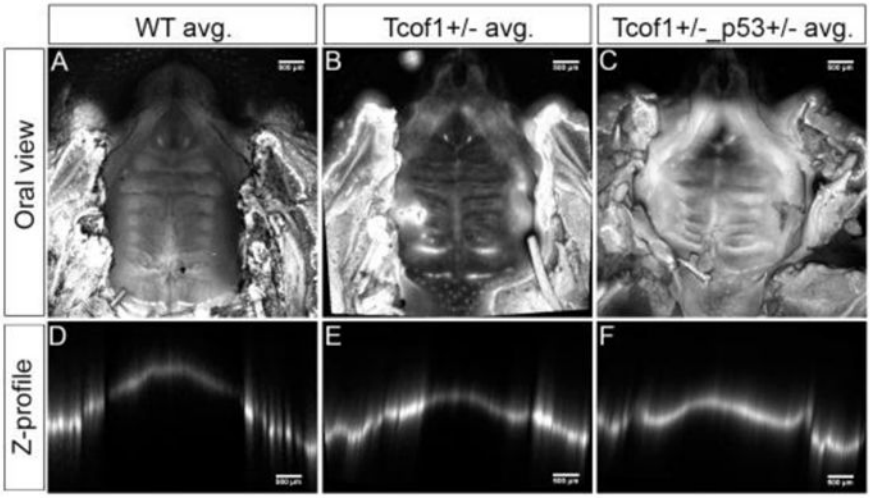

Figure 7.

Representative oral views of maximum intensity fluorescent confocal projections of DAPI stained (A) wild-type, (B) $Tcof1^{+/-}$, and (C) $Tcof1^{+/-}$;$Trp53^{+/-}$ palates, with their respective Z-stack profiles (D–F).

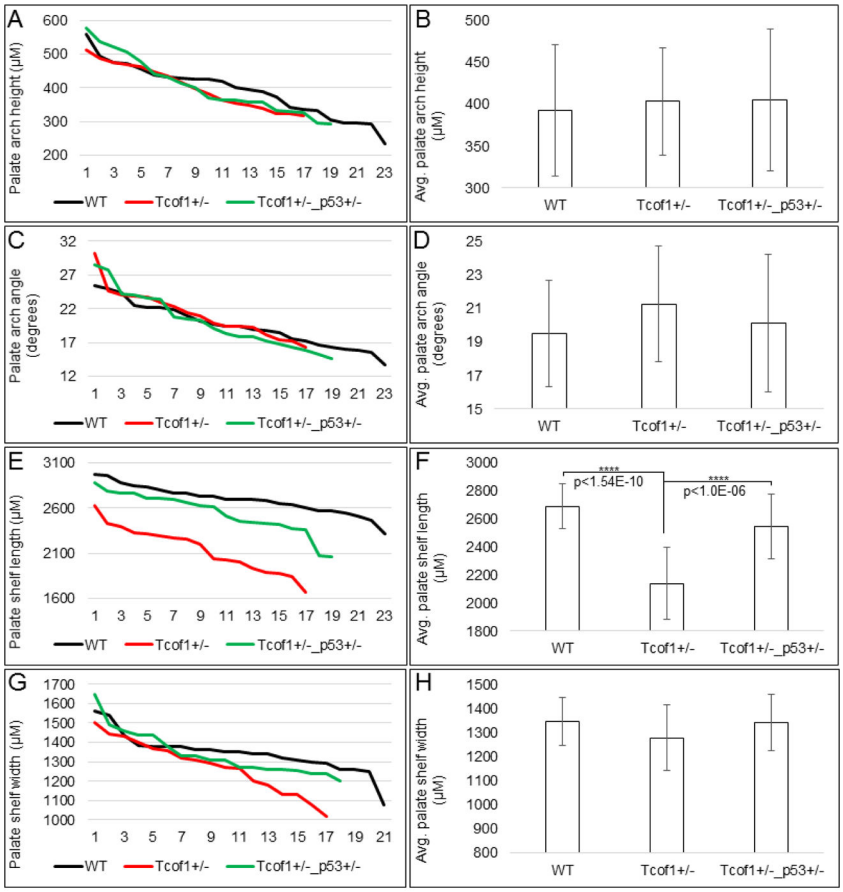

Figure 8.

Analyses of palate arch height (A, B),angle (C,D), shelf length (E, F) and shelf width (G, H) measurements in wild-type, Tcof1$^{+/-}$ and Tcof1$^{+/-}$;Trp53$^{+/-}$ embryos and pups. Samples were plotted from greatest to least magnitude (A, C, E, and G). Bar graphs (B, D, F, H) represent the averages and standard deviations of wild-type, Tcof1$^{+/-}$, and Tcof1$^{+/-}$;Trp53$^{+/-}$ palate arch height, arch angle, shelf length, and shelf width sets, respectively.